RSC Advances

PAPER

View Article Online
View Journal | View Issue

Cite this: *RSC Adv.*, 2021, **11**, 14071

Production of cellulose nanofibrils and films from elephant grass using deep eutectic solvents and a solid acid catalyst†

Xi-Que Wu,[a] Pan-Dao Liu,[b] Qun Liu,[a] Shu-Ying Xu,[a] Yu-Cang Zhang,[c] Wen-Rong Xu *[a] and Guo-Dao Liu*[b]

Received 22nd March 2021
Accepted 6th April 2021

DOI: 10.1039/d1ra02259h

rsc.li/rsc-advances

A new strategy was developed to produce cellulose nanofibrils (CNFs) and films from raw elephant grass using deep eutectic solvents and a recyclable spent coffee-derived solid acid (SC-SO_3H) catalyst with assistance of ultrasonic disintegration and a suction filtration film forming method. The effects of a solid acid and reused solid acid were comprehensively studied by comparing with catalyst-free conditions and using sulfuric acid as the catalyst. The CNF fibers obtained from this novel SC-SO_3H catalyst method showed the longest fiber length. The corresponding films achieved the strongest tensile strength of 79.8 MPa and the elongation at break of 13.6%, and best thermostability. In addition, the performance of CNFs and films prepared by the fourth recovered SC-SO_3H-4 catalyst was close to that obtained with the first use. The SC-SO_3H could be reused by a simple decantation method, meaning this novel method has the potential for green and sustainable preparation of CNFs and films.

Introduction

The development of green, sustainable and biodegradable materials has received increasing attention due to the gradual depletion of fossil resources and the concern for environmental sustainability. Biodegradable polymers are considered as potential alternatives to petroleum-based products, among which cellulose is the most popular for its abundance, and renewable and non-toxic properties.[1] Cellulose nanofibrils (CNFs) have a typical width of 3–100 nm and a length of several hundred nanometers to several micrometers. CNFs have the advantages of high specific surface area, high strength and stiffness, low density and a low thermal expansion coefficient, which lead to potential value-added applications in fields such as biomedicine engineering, food, sensors, packaging, and optical and electronic devices.[2] The production of CNFs from wood or plant biomass is challenging because cellulose is encapsulated in a matrix of lignin and hemicellulose with a compact and complex hierarchy structure in plant cell walls.[3] The most common approach to produce CNFs usually requires first removing the non-cellulose components and bleaching the residues through alkaline and acid-chlorite treatments.[4] Then, the extracted cellulose is mainly degraded by mineral acid hydrolysis pretreatment combined with mechanical disintegration to provide CNFs.[5] However, such approach is not very environmentally friendly because of the difficulties in economically recovering acids and bases and the requirement for disposal of large amounts of salt from neutralization.[6] Solid acid is an emerging catalyst with its various advantages such as high activity, recyclability and less hazards to equipment.[7] In the extraction and nanoprocessing of cellulose, the problem of acid recycling can be solved by using solid acid instead of mineral acid.[8]

In recent years, a new class of green chemicals termed deep eutectic solvents (DESs) have received widespread attention, as they can play as solvents, reactants and catalysts for pretreatment and conversion of biomass.[9] DESs are commonly formed by mixing a halide salt of a quaternary ammonium or a phosphonium cation that acts as a hydrogen bond acceptor (HBA), along with a hydrogen bond donor (HBD), such as polyols, urea, carboxylic acids and metal salts.[10] They own the characteristics of high dissolution capacity, high chemical and thermal stability, low vapor pressure, easy preparation, facile recycling, non-toxicity, biodegradability and low cost, making them green chemicals for lignocellulose pretreatment to prepare CNFs.[11] However, most of the reported studies using DESs to prepare CNFs have used the bleached cellulose pumps[12] or biomass with high cellulose content (larger than 60%)[13] as starting materials. The production of good qualities of CNFs and films from raw biomass (cellulose content smaller than 60%) by merely DESs pretreatment is still an elusive challenge.

[a]*Key Laboratory of Advanced Materials of Tropical Island Resources of Ministry of Education, Hainan Provincial Key Laboratory of Fine Chemistry, Key Laboratory of Solid Waste Resource Utilization and Environmental Protection, School of Science, School of Chemical Engineering and Technology, Hainan University, Haikou 570228, PR China. E-mail: xuwr2016@hainanu.edu.cn*

[b]*Institute of Tropical Crop Genetic Resources, Chinese Academy of Tropical Agriculture Sciences, Haikou 571101, PR China. E-mail: Guodao_Liu@163.com*

[c]*College of Food and Biological Engineering, Jimei University, Xiamen 361021, PR China*

† Electronic supplementary information (ESI) available. See DOI: 10.1039/d1ra02259h

Elephant grass (*Pennisetum purpureum*) is an important forage, biofuel and industrial plant that widely distributed in tropical and subtropical regions around the world. It is considered one of the most prospective energy crops due to its robust growth, high biomass productivity, strong carbon sequestration ability, high adaptability and low nutrient requirements.[14] The cellulose content of elephant grass stalks had been investigated earlier as 40.3%, which was higher than most straws, such as reed straw, wheat straw and corn stover.[15] This determines that elephant grass is a promising plant for cellulose extraction and cellulose nanomaterial production. In previous studies, Rezende *et al.* reported a conventional alkali and acid pretreatment method to obtain cellulose nanofibrils (3.8–9.7%, w/w yield), together with nanocrystals (12–16%, w/w yield) from elephant grass leaves.[16]

In this study, the stalk of elephant grass was used as raw material to extract cellulose by pretreatments of DESs and spent coffee-derived solid acid (SC-SO_3H) catalyst. The effects of SC-SO_3H and reused SC-SO_3H were comprehensively studied by comparing with catalyst-free condition and sulfuric acid as catalyst condition. The cellulose obtained under different conditions was characterized by FTIR, XRD and SEM, and subsequently converted into CNFs by ultrasonic disintegration. The morphology of CNFs was observed by TEM investigation. In addition, the CNF samples were prepared into films by vacuum filtration. The morphology, mechanical and thermal properties of the CNF films were characterized.

Materials and methods

Materials

Elephant grass (*Pennisetum purpureum*) stalks harvested for 2 months were provided by the Chinese Academy of Tropical Agriculture Sciences (Haikou, China). The stalks were dried in an oven at 60 °C for 24 h, then crushed with a multifunctional crusher (YB-2500A, China Shufeng) and passed through a 120-mesh sieve to obtain elephant grass stalk powder. Choline chloride was purchased from Aladdin Co., Ltd. Sulfuric acid (95–98%) and glycerol were purchased from Xilong Chemical Co., Ltd. Oxalic acid dihydrate and sodium chlorite were purchased from Aladdin Co., Ltd. The spent coffee-derived solid acid catalyst (SC-SO_3H) was prepared according to our previous report method.[17]

Synthesis of DESs

Choline chloride (ChCl) and glycerol were mixed in a ratio of 1 : 2 and heated at 90 °C in an oil bath with continuous magnetic stirring for 60 min to afford a transparent and homogeneous DES-1: ChCl–glycerol. Choline chloride and oxalic acid dihydrate were mixed in a ratio of 1 : 1 at 60 °C with continuous magnetic stirring for 60 min to give DES-2: ChCl–oxalic acid dihydrate.

Extraction and purification of elephant grass cellulose

The schematic illustration of extraction and purification of cellulose from elephant grass is shown in Fig. 1, which was primarily divided into three steps:

(i) DES-1 and SC-SO_3H treatment: a mixture of elephant grass powder (EG, 1.0 g) and ChCl–glycerol (1 : 2, 20.0 g) was magnetic stirred at 140 °C for 30 min. Then SC-SO_3H (0.3 g) was added and the mixture was further stirred at 140 °C for 3 h. After the reaction was cooled, a mixed solvent of 1,4-dioxane and water (4 : 1, v/v, 50 mL) was added, and the SC-SO_3H was settled to the bottom, and subsequently separated from the suspension by decantation. The collected SC-SO_3H was dried in an oven at 60 °C for 24 h and could be recycled without further treatment. The resulting suspension was filtered by suction filtration and washed with the mixed solvent of 1,4-dioxane and water to give a pale yellow powder.

(ii) Bleaching: the pale yellow powder was further bleached with 7 wt% $NaClO_2$ aqueous solution at 90 °C for 4 h, and then washed with deionized water and dried to obtain a white crude cellulose (0.31 g).

(iii) DES-2 treatment: the crude cellulose and ChCl–oxalic acid dihydrate (1 : 1, 31.0 g) was stirred at 80 °C for 3 h. The suspension was then suction filtrated and washed with deionized water. The residue was dried in oven at 60 °C for 24 h to

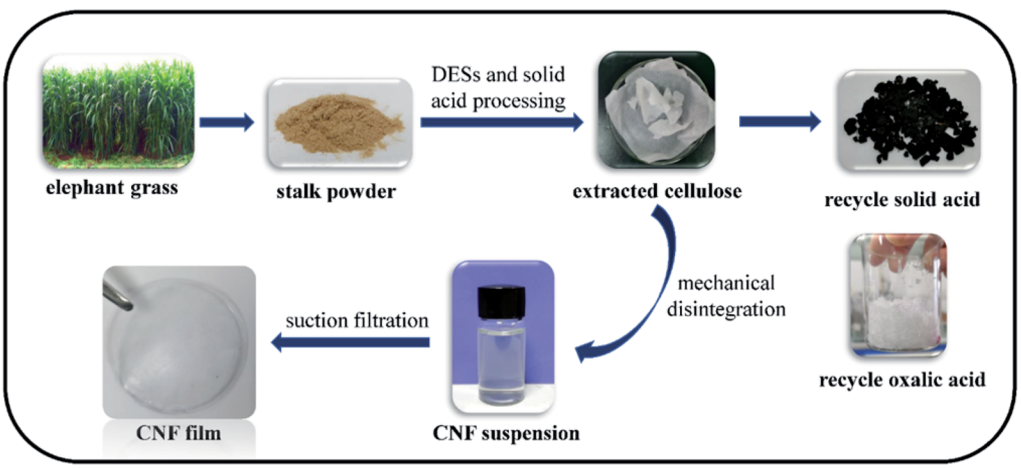

Fig. 1 Schematic illustration for the production of CNFs and films from elephant grass.

afford purified cellulose (0.25 g). The filtrate was subjected to rotary evaporation at 80 °C to remove water. The remaining solution was recrystallized and filtered to obtain the recovered oxalic acid dihydrate as a white solid.

The purified cellulose prepared with SC-SO_3H as a catalyst was named SCC, and the corresponding cellulose obtained by using SC-SO_3H for the second, third and fourth recycling were named SCC-2, SCC-3 and SCC-4, respectively.

The comparative experiments were carried out by following the above procedures without adding SC-SO_3H as a catalyst (blank), or using sulfuric acid (0.2 mL for 1.0 g elephant grass powder) as a catalyst instead of SC-SO_3H to prepare cellulose. The obtained cellulose under these two conditions were named BLC and H_2SO_4–C, respectively. Each reaction sequence was repeated three times.

The yield of cellulose isolated from elephant grass was calculated by the following formula:

$$\text{Yield } (\%) = (G_2/G_1) \times 100\% \quad (1)$$

in which G_1 and G_2 are the quantity of the raw material EG and the extract cellulose, respectively.

Chemical composition analysis

Klason lignin and ash contents were measured according to TAPPI standard methods TAPPI T222 om-06 (2006) and TAPPI T211 om-07 (2007), respectively. The carbohydrates composition was analyzed according to the method described by Theander and Westerlund (1986).

Preparation of elephant grass cellulose nanofibrils

The purified cellulose (0.02 g) was dispersed in deionized water (80 mL), and then the suspension was subjected to 3 h of ultrasonication using an Ultrasonic Processor (JY98-IIIL, 20 kHz, 1000 W, Dekelaier, China) equipped with a cylindrical titanium alloy probe (20 mm in diameter). A double wall glass crushing cup with a recirculating cooling system (LX-300, Changliu, China) setting at 4 °C was used to keep the solution cool. Transparent suspensions of CNF (0.025 wt%) were obtained, which were stored at 4 °C for future use.

Preparation of cellulose nanofibril films

A sand core funnel equipped with a mixed cellulose ester membrane filter with a pore size of 0.22 μm and a diameter of 90 mm was used to vacuum filter the suspension of cellulose nanofibrils to obtain CNF films. After filtration, the film was sandwiched between filter papers, which was then placed between two glass plates at room temperature for 12 h. The dried film was peeled off carefully and its thickness was further measured to be 43 ± 2 μm.

Fourier transform infrared spectroscopy

The structure of EG and cellulose obtained under different conditions including BLC, H_2SO_4–C, SCC and SCC-4 were characterized by Fourier transform infrared spectroscopy (FTIR) analysis on a Bruker TENSOR27 spectrometer using the KBr-disk method. The concentration of each sample in KBr was 0.25%. The spectra were recorded in the range of 4000–500 cm^{-1} with a resolution of 4 cm^{-1} and 32 scans. All the spectra were normalized at 3445 cm^{-1}.

X-ray diffraction analysis

The X-ray diffraction (XRD) patterns of EG and extracted cellulose were recorded on a Bruker D8 Advance X-ray diffractometer using CuKα radiation at 40 kV. The measurement was performed in the range of $2\theta = 10°$ to 30° at a scanning rate of 4° min^{-1}. The crystallinity index (CrI) was calculated by using Segal formula as eqn (2).

$$\text{CrI } (\%) = [(I_{002} - I_{am})/I_{002}] \times 100\% \quad (2)$$

Morphology characterization

Scanning electron microscopy (SEM) was used to observe the surface morphology of EG, extracted cellulose, as well as the surfaces and cross sections of CNF films. SEM observation was conducted using a scanning electron microscopy (Phenom ProX, Holland) operating at 30 kV.

The morphology of CNFs was characterized by using a transmission electron microscope (TEM, JEM-1200EX, Japan). The test sample was negatively stained with uranyl acetate, and micrographs were recorded at an acceleration voltage of 120 kV. The diameter of CNFs was calculated according to the reported method.[18]

Thermal characterization

Thermogravimetric analysis of CNF films was performed on a METTLER TOLEDO DSC 3+ thermogravimetric analyzer under a nitrogen atmosphere with a temperature range of 30 °C to 800 °C at a heating rate of 10 °C min^{-1}.

Mechanical property characterization

The determination of tensile strength and elongation at break of CNF films was carried out on a universal testing machine (INSTRON-3343) at a speed rate of 0.1 mm min^{-1}. The specimens were cut into dumbbell shapes with a length of 35 mm and a width of 2 mm. Each sample was tested for three times and the average values and standard deviations were calculated.

Result and discussion

Chemical components of elephant grass and isolated cellulose

Choline-based DESs were reported as effective reagents for separating cellulose from lignocellulose. For example, ChCl–glycerol, ChCl–urea and ChCl–ethylene glycol can dissolve lignin, while ChCl–oxalic acid can effectively separate lignin and hemicellulose.[19] In this study, a three-step method was developed to isolate cellulose from elephant grass. Firstly, ChCl–glycerol DES-1 was used in combination with the solid acid SC-SO_3H catalyst derived from spent coffee to remove

Table 1 Chemical components of raw EG and cellulose BLC, H_2SO_4–C, SCC and SCC-4

Samples	Catalyst	Cellulose (%)	Hemicellulose (%)	Kraft lignin (%)	Ash (%)	Yield of cellulose (%)
EG	—	40.5	23.0	17.8	3.7	—
BLC	—	76.2	13.4	5.9	1.2	28.2
H_2SO_4–C	H_2SO_4	85.5	5.6	6.7	0.9	19.2
SCC	SC-SO_3H	79.3	11.7	2.4	0.5	25.0
SCC-4	SC-SO_3H-4	76.6	11.1	4.1	1.3	27.3

lignin. The SC-SO_3H was used to enhance the removal ability of lignin. After the second bleaching step, the residue was further treated with ChCl–oxalic acid DES-2 to remove lignin and hemicellulose. Recent reports indicate that the DES decomposes and/or evaporates during high-temperature heating.[20] Therefore, DES should be prepared and applied below the decomposition temperature (*i.e.*, 175.5 °C of DES-1 and 162.1 °C of DES-2).[20a] During the heating process of DESs preparation and cellulose extraction, a water condenser was equipped to reduce the possible evaporation of DESs. In order to evaluate the effect of SC-SO_3H, comparative experiments were carried out without adding SC-SO_3H and using H_2SO_4 instead of SC-SO_3H as a catalyst. The chemical components of raw EG and cellulose separated under different conditions are listed in Table 1. The cellulose, hemicellulose, lignin and ash contents of elephant grass were measured to be 40.5%, 23.0%, 17.8% and 3.7%, respectively. After DESs treatments under different catalyst conditions, the cellulose content increased significantly. The H_2SO_4–C showed the highest cellulose content of 85.5%, but the lowest yield of 19.2%. The low cellulose yield might be attributed to the unavoidable degradation of cellulose chains into water-soluble sugar oligomers under strong acidity of sulfuric acid.[7b] In addition, the color of H_2SO_4–C appeared yellowish (Fig. 4a), which might be due to a small amount of carbonization of lignocellulose under heated sulfuric acid conditions. In contrast, SCC had a slightly lower cellulose content of 79.3%, but a higher yield of 25.1%. Particularly, the cellulose content of SCC-4 extracted by the fourth cycle of SC-SO_3H was 76.6%, which was a little lower than that of SCC, but still higher than that of BLC. Moreover, the hemicellulose and lignin contents of SCC-4 were all moderately lower than those of BLC, indicating that the solid acid used repeatedly for the fourth time still had a certain catalytic effect. Comprehensive consideration, the combined use of SC-SO_3H and DESs was an effective method to separate cellulose from elephant grass.

FTIR spectroscopy of elephant grass and isolated cellulose

The FTIR spectra of EG and celluloses isolated with different pretreatments are shown in Fig. 2a. In the EG spectrum, the broad peak at 3445 cm^{-1} reflected the O–H stretching vibration of hydroxyl groups, while the vibrations at 2925 and 2855 cm^{-1} corresponded to saturated C–H stretching vibrations of methyl and methylene groups.[21] The band around 1745 cm^{-1} was ascribing to the C=O stretching vibration of acetyl groups in lignin and ester groups in hemicelluloses.[22] The band around 1635 cm^{-1} was assigned to the O–H bending of water absorbed in cellulose fiber. The absorptions at 1514 cm^{-1} and 1250 cm^{-1} arose from the aromatic C=C stretching of aromatic ring and the C–O stretching in lignin,[13b] respectively. The absorptions at 1745 cm^{-1}, 1514 cm^{-1} and 1250 cm^{-1} of BLC were obviously weakened, indicating that the amounts of hemicellulose and lignin were reduced after DESs pretreatment. The peak at 1745 cm^{-1} and 1514 cm^{-1} were further reduced at the spectrum of H_2SO_4–C, which was regarded as the reduction of the lignin amount with sulfuric acid catalyst combined with DESs pretreatment. The disappearance of absorption bands at 1745 cm^{-1}, 1514 cm^{-1} and 1250 cm^{-1} of SCC, SCC-4 indicated the removal of most hemicellulose and lignin. The FTIR results were basically in accordance with the component analysis results.

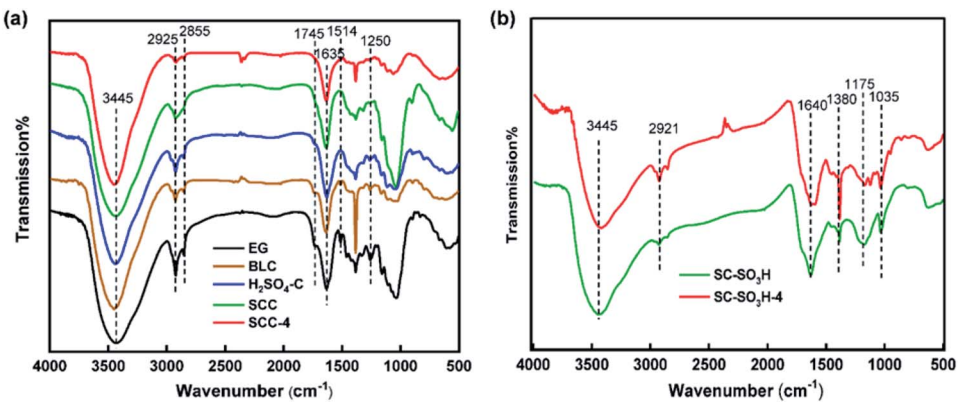

Fig. 2 (a) FTIR spectra of EG, BLC, H_2SO_4–C, SCC and SCC-4; (b) FTIR spectra of SC-SO_3H and SC-SO_3H-4.

The FTIR spectra of SC-SO_3H and SC-SO_3H-4 after the fourth cycle are displayed in Fig. 2b. The broad peak around 3445 cm^{-1} was ascribed to the O–H stretching vibration in phenolic hydroxyl groups. The small absorption at 2921 cm^{-1} was assigned to C–H. The peaks at 1640 cm^{-1} and 1380 cm^{-1} were assigned to the C=C stretching and aromatic C–O stretching.[17] The peaks around 1380 cm^{-1} (overlapped with C–O stretching), 1175 cm^{-1} and 1035 cm^{-1} were ascribed to O=S=O stretching vibration of SO_3H groups.[23] The peaks at 2921 cm^{-1}, 1640 cm^{-1} and 1380 cm^{-1} were slightly enhanced, which suggested that a small amount of lignocellulose might be linked to the solid acid. On the contrary, the peaks at 1175 cm^{-1} and 1035 cm^{-1} were slightly reduced, which indicated that some of the active SO_3H groups in the reused solid acid had been consumed, leading to a gradual decrease in catalytic activity.

The recovery and recycling of DESs can be effectively achieved by reported methods, such as rotary evaporation,[24] ultrafiltration and electrodialysis.[15] In this work, we didn't intend to study the recovery of DESs, but we unexpectedly discovered that the oxalic acid dihydrate in DES-2 could be easily recovered by recrystallization from the filtrate after removing the cellulose residue. The recovered oxalic acid dihydrate appeared as a white solid (Fig. 1) with high purity, and its structure was characterized by FTIR spectroscopy (Fig. S1†), ^{1}H NMR and ^{13}C NMR spectroscopy (Fig. S2†), which were consistent with the data of standard sample.

X-ray diffraction analysis of elephant grass and isolated cellulose

The X-ray diffraction patterns of EG, BLC, H_2SO_4–C, SCC and SCC-4 are depicted in Fig. 3. The samples displayed two main peaks around 16° and 22°, which were attributed to the planes of (110) and (200), respectively.[25] This indicated that the cellulose obtained by these pretreatments still remained in the type of cellulose I allomorph. The crystallinity of raw EG was calculated to be 47.4%. After various treatments, the crystallinity of BLC, H_2SO_4–C, SCC and SCC-4 were significantly increased to 72–74% due to the effective elimination of amorphous portions typically composed of lignin and hemicellulose.[26]

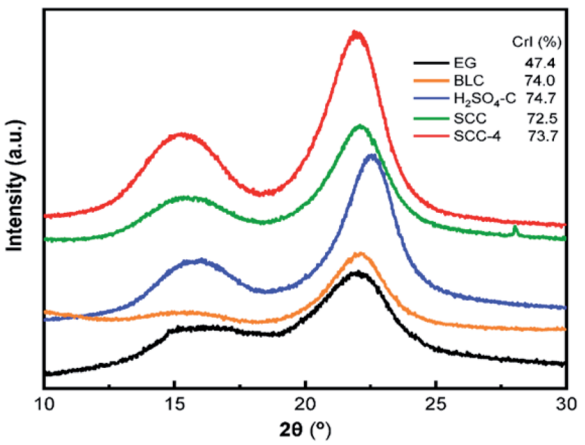

Fig. 3 X-ray diffraction patterns of EG, BLC, H_2SO_4–C, SCC and SCC-4.

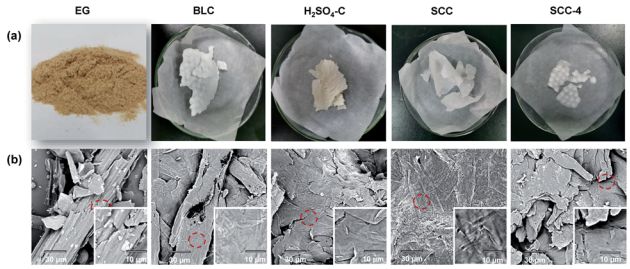

Fig. 4 (a) Optical and (b) SEM images of EG, BLC, H_2SO_4–C, SCC and SCC-4.

Morphology of cellulose and CNFs

The optical images of EG and isolated cellulose under different conditions are displayed in Fig. 4a. BCL, SCC and SCC-4 presented as white, while the H_2SO_4–C showed as yellowish. The corresponding SEM images (Fig. 4b) demonstrated that the surface of all isolated cellulose was smoother than that of EG, which was due to the removal of hemicellulose and lignin from EG by pretreatments.[27] Moreover, the hollow rod in BLC was destroyed by additional sulfuric acid or SC-SO_3H catalyst, as in H_2SO_4–C, SCC and SCC-4.

After ultrasonic treatment, the suspension of CNFs (0.025 wt%) all appeared completely transparent (Fig. 5e). The sonicated suspension of SCC (namely SCCNF) could stand stably for at least 15 days without sedimentation, which should be caused by its inherent repulsive forces as its zeta potential was measured to be −39.45 mV.[28] Moreover, all transparent CNF suspensions exhibited clear Tyndall effects (Fig. 5e), indicating the existence of abundant nanostructures.[29] Transmission electron microscopy (TEM) was used to study the morphology and size distribution of the CNFs. As shown in the TEM images (Fig. 5a–d), the BLCNF, SCCNF and SCCNF-4 nanofibrils showed a hairy and network structures, especially the latter two because they held the longest filament length of about 800 to 1000 nm, while the length of BLCNF nanofibrils were about 400

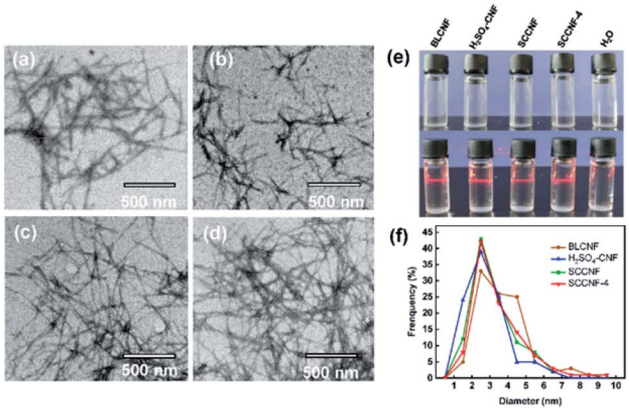

Fig. 5 TEM images of (a) BLCNF, (b) H_2SO_4–CNF, (c) SCCNF and (d) SCCNF-4; (e) images of different CNF suspensions (upper) and the corresponding Tyndall effects (down); (f) the diameter distributions of CNFs.

to 700 nm. In contrast, the H_2SO_4–CNF nanofibrils appeared the shortest length ranging from 150 to 250 nm, but more precisely, it was closer to nanocrystals. The formation of nanocrystalline structures of H_2SO_4–CNF might be due to the excessive hydrolysis degree of cellulose under strong acid condition. Moreover, the nanocrystalline of H_2SO_4–CNF aggregated into small bundles. The diameter distribution of CNFs was obtained on the basis of statistical calculation of 100 fibers randomly selected from the TEM image of CNFs. The results in Fig. 5f demonstrated that the diameters of CNFs were very close, distributed in the range of 2 to 6 nm, which were smaller than the elephant grass nanocellulose obtained in the previous report.[16] It should be noted that the diameter distributions of SCCNF and SCCNF-4 were extremely similar, which suggested the effectiveness of the recovered solid acid catalyst.

Morphology of CNF films

After the CNF suspensions were subjected to suction filtration and drying process, CNF films were obtained. As shown in Fig. 6a, except for H_2SO_4–CNF-f film which showed a very slight yellow color, all other CNF films were colorless and transparent. The SEM observation showed that the nanoparticles on the surfaces of the SCCNF-f and SCCNF-f-4 films were better dispersed than those of BLCNF-f and H_2SO_4–CNF-f films in scope (Fig. 6b). The cross-sections (Fig. 6c) of all CNF films showed a multilayer structure, which was similar to previously reported CNF films obtained by suction filtration method.[30] In addition, the cross-sections of SCCNF-f and SCCNF-f-4 films were more uniform and compact than the cross-sections of BLCNF-f and H_2SO_4–CNF-f films. The latter two showed chaotic stratification and small aggregations, respectively. The better smoothness and uniformity of SCCNF-f and SCCNF-f-4 films were owing to the more uniform size of their corresponding CNFs, as verified by TEM results.

Mechanical property of CNF films

The tensile strength and elongation at break of BLCNF-f, H_2SO_4–CNF-f, SCCNF-f and SCCNF-f-4 films with the thickness of 43 ± 2 μm were measured. As shown in Fig. 7, H_2SO_4–CNF-f film displayed the lowest tensile strength and elongation at break of 44.2 MPa and 5.4%, respectively. Even though, it was still superior to the reported values of pure CNF film.[31] The relatively weak mechanical property of H_2SO_4–CNF-f film might be due to the excessive hydrolysis degree of cellulose under strong acid condition and the uneven aggregation of CNFs in the film. As expected, SCCNF-f film showed the best mechanical property with the tensile strength and elongation at break of 79.8 MPa and 13.6%, respectively. This behavior should be attributed to its well-dispersed and long CNF fibers, as long fibers were more easily entangled with each other though intermolecular hydrogen bonding.[32] The tensile strength of the SCCNF-f-4 film derived from the repeated use of SC-SO_3H-4 catalyst was slight reduced to 77.5 MPa, and the elongation at break was decreased to 9.3%, but the values were still better than those of BLCNF-f film (72.8 MPa, 9.4%).

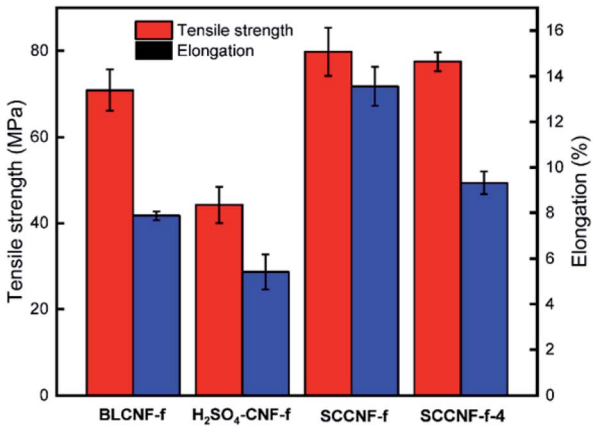

Fig. 7 Tensile strength and elongation at break of BLCNF-f, H_2SO_4–CNF-f, SCCNF-f and SCCNF-f-4 films.

Thermal stability of CNF films

Thermogravimetric (TGA) and derivative thermogravimetric (DTG) analyses were carried out to detect the thermal stability of different CNF films. As presented in Fig. 8, all film showed

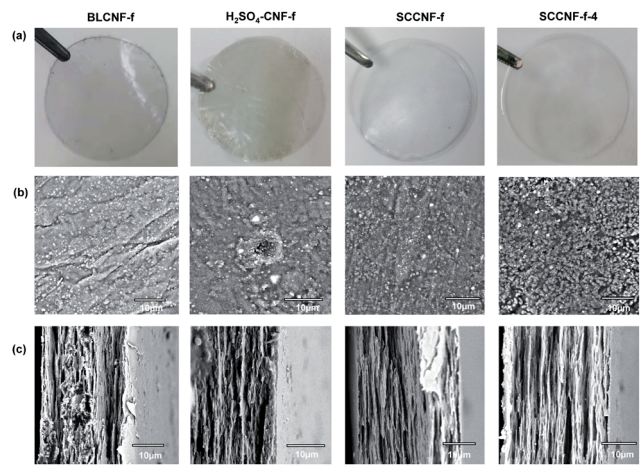

Fig. 6 (a) Optical images of CNF films; SEM images of (b) the surface and (c) the cross-section of CNF films.

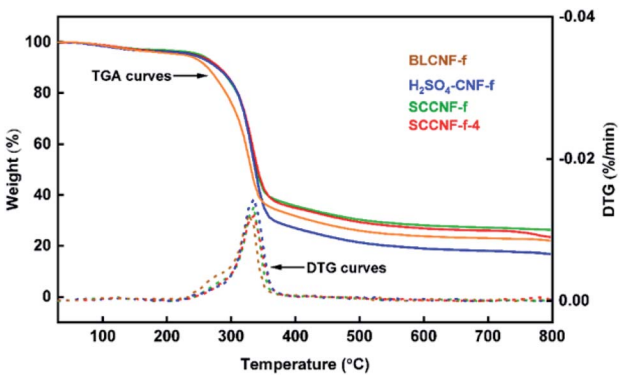

Fig. 8 TGA and DTG curves of BLCNF-f, H_2SO_4–CNF-f, SCCNF-f and SCCNF-f-4 films.

a slight weight loss at low temperature range of 70–125 °C due to evaporation of absorbed and intermolecular hydrogen bonded moisture.[33] In the TGA curves presented by weight (%) and solid line, the apparent weight loss of the BLCNF-f film began at 234 °C, while the other three films began at a higher temperature of 257 °C under nitrogen atmosphere. From the DTG curves shown by the dotted line, it can be seen that all H_2SO_4–CNF-f, SCCNF-f and SCCNF-f films exhibited a prominent pyrolysis process with mainly single degradation and the accompanying weight loss mostly occurred at 257–375 °C. Whereas, the significant pyrolysis of the BLCNF-f film took place in a relatively low temperature range of 242–359 °C, and was accompanied by an obvious shoulder around 242–296 °C. The shoulder peak might be triggered by the degradation of hemicellulose since its lower thermal stability compared with lignin and cellulose,[34] and the BLCNF-f was speculated to have the highest hemicellulose content in all samples from the composition results in Table 1. In all curves, the weight loss in the temperature range of about 300–375 °C should be attributed to the decomposition of lignin and cellulose.[21a]

It was worth noting that the thermal degradation curves of SCCNF-f and SCCNF-f-4 films were similar. Both of them possessed the highest thermal stability with a maximum degradation temperature (T_{max}) at 336 °C with 43% weight loss. But their char residue content at 800 °C was slightly different, which was 26% and 23%, respectively. While the H_2SO_4–CNF-f film showed the same T_{max} at 336 °C, but its weight loss (47%) was slightly higher than those of SCCNF-f and SCCNF-f-4 films, and its amount of char residue at 800 °C was low to 17%. The reason should be ascribed to the longer length of fibers[35] in SCCNF-f and SCCNF-f-4 films. These results suggested that the CNF films produced from fibers treated with solid acid catalyst occupied the best thermal stability.

Conclusions

CNFs were successfully prepared by using DESs under different catalysts combined with ultrasonically disintegration from raw elephant grass, and the corresponding CNF films were obtained by suction filtration. The CNFs derived from SC-SO_3H treatments showed the best dispersibility and uniform size with a diameter distribution in 2 to 6 nm and length in 800 to 1000 nm, and the corresponding CNF films showed the best mechanical and thermal properties. The recovered SC-SO_3H catalysts still maintained good performance, even in the fourth cycle of use, the isolated cellulose, CNFs and films still showed close characteristics to the first use. The CNFs and films produced by these novel DESs and solid acid method may have potential application in the fields such as bioplastics, optical and electronic devices.

Author contributions

Xi-Que Wu: investigation, methodology, verification, writing – original draft; Pan-Dao Liu: resources, funding acquisition; Qun Liu: resources; Shu-Ying Xu: formal analysis; Yu-Cang Zhang: funding acquisition; Wen-Rong Xu: conceptualization, writing – review & editing, supervision, funding acquisition; Guo-Dao Liu: conceptualization, resources, project administration, funding acquisition.

Conflicts of interest

The authors declare that no competing interests.

Acknowledgements

This work was supported by the Key Scientific Research Project Funding of Hainan Province (No. ZDYF2020184), National Natural Science Foundation of China (No. 22061015, No. 21978059), Young Elite Scientists Sponsorship Program by CAST (No. 2019QNRC001) and Modern Agro-industry Technology Research System (No. CARS-34).

References

1 (*a*) H. P. S. Abdul Khalil, A. H. Bhat and A. F. Ireana Yusra, *Carbohydr. Polym.*, 2012, **87**(2), 963; (*b*) O. Nechyporchuk, M. N. Belgacem and J. Bras, *Ind. Crops Prod.*, 2016, **93**, 2.

2 (*a*) B. Deepa, E. Abraham, B. M. Cherian, A. Bismarck, J. J. Blaker, L. A. Pothan, A. L. Leao, S. F. de Souza and M. Kottaisamy, *Bioresour. Technol.*, 2011, **102**(2), 1988; (*b*) L. Long, D. Tian, J. Hu, F. Wang and J. Saddler, *Bioresour. Technol.*, 2017, **243**, 898; (*c*) J. T. Xu and X. Q. Chen, *Bioresour. Technol.*, 2019, **291**, 121842.

3 J. Wang, Q. Wang, Y. Wu, F. Bai, H. Wang, S. Si, Y. Lu, X. Li and S. Wang, *Nanomaterials*, 2020, **10**(11), 2227.

4 P. Phanthong, P. Reubroycharoen, X. Hao, G. Xu, A. Abudula and G. Guan, *Carbon Resour. Convers.*, 2018, **1**(1), 32.

5 (*a*) H. V. Lee, S. B. Hamid and S. K. Zain, *Sci. World J.*, 2014, 631013; (*b*) H. Xie, H. Du, X. Yang and C. Si, *Int. J. Polym. Sci.*, 2018, 923068.

6 (*a*) L. Chen, J. Y. Zhu, C. Baez, P. Kitin and T. Elder, *Green Chem.*, 2016, **18**(13), 3835; (*b*) A. K. Kumar and S. Sharma, *Bioresour. Bioprocess.*, 2017, **4**(7), 1.

7 (*a*) S. Hu, F. Jiang and Y.-L. Hsieh, *ACS Sustainable Chem. Eng.*, 2015, **3**(10), 2566; (*b*) K. Song, Y. Ji, L. Wang, Y. Wei and Z. Yu, *J. Cleaner Prod.*, 2018, **196**, 1169.

8 Y. Zhao, H. Lei, Y. Liu, R. Ruan, M. Qian, E. Huo, Q. Zhang, Z. Huang, X. Lin, C. Wang, W. Mateo and E. M. Villota, *Sci. Total Environ.*, 2020, **731**, 138751.

9 (*a*) Y. Chen and T. Mu, *Green Energy Environ.*, 2019, **4**(2), 95; (*b*) T. Suopajärvi, P. Ricci, V. Karvonen, G. Ottolina and H. Liimatainen, *Ind. Crops Prod.*, 2020, **145**, 111956.

10 (*a*) J. A. Sirviö, M. Visanko and H. Liimatainen, *Green Chem.*, 2015, **17**(6), 3401; (*b*) X. Tang, M. Zuo, Z. Li, H. Liu, C. Xiong, X. Zeng, Y. Sun, L. Hu, S. Liu, T. Lei and L. Lin, *ChemSusChem*, 2017, **10**(13), 2696.

11 (*a*) P. Li, Y. Wang, Q. Hou, H. Liu, H. Lei, B. Jian and X. Li, *Cellulose*, 2020, **27**(5), 2511; (*b*) S. Liu, Q. Zhang, S. Gou, L. Zhang and Z. Wang, *Carbohydr. Polym.*, 2021, **251**, 117018; (*c*) K. Nomura and P. Terwilliger, *Spec. Matrices*, 2019, **8**(1), 568.

12 (*a*) P. Li, J. A. Sirvio, A. Haapala and H. Liimatainen, *ACS Appl. Mater. Interfaces*, 2017, **9**(3), 2846; (*b*) J. A. Sirviö, M. Visanko, J. P. Heiskanen and H. Liimatainen, *J. Mater. Chem.*, 2016, **4**(17), 6368.

13 (*a*) I. M. De Rosa, J. M. Kenny, M. Maniruzzaman, M. Monti, D. Puglia, C. Santulli and F. Sarasini, *Compos. Sci. Technol.*, 2011, **71**(2), 246; (*b*) W. Yu, C. Wang, Y. Yi, H. Wang, L. Zeng, M. Li, Y. Yang and Z. Tan, *ACS Omega*, 2020, **5**, 5580; (*c*) X. Tan, W. Zhao and T. Mu, *Green Chem.*, 2018, **20**, 3625; (*d*) X. Tan, Y. Wang, W. Du and T. Mu, *ChemSusChem*, 2020, **13**(2), 321.

14 V. Strezov, T. J. Evans and C. Hayman, *Bioresour. Technol.*, 2008, **99**(17), 8394.

15 X. Liang, Y. Fu and J. Chang, *Sep. Purif. Technol.*, 2019, **210**, 409.

16 S. A. Nascimento and C. A. Rezende, *Carbohydr. Polym.*, 2018, **180**, 38.

17 Q. Liu, Z. Zhai, J. Guo, J. Cheng and Y. Zhang, *Carbohydr. Polym.*, 2021, **254**, 117427.

18 J. Han, C. Zhou, Y. Wu, F. Liu and Q. Wu, *Biomacromolecules*, 2013, **14**(5), 1529.

19 C. Li, C. Huang, Y. Zhao, C. Zheng, H. Su, L. Zhang, W. Luo, S. Zhao, S. Wang and L.-J. Hunag, *Processes*, 2021, **384**, 1.

20 (*a*) W. Chen, Z. Xue, J. Wang, J. Jiang, X. Zhao and T. Mu, *Acta Phys.-Chem. Sin.*, 2018, **34**(8), 904; (*b*) Y. Chen, Q. Wang, Z. Liu, W. Chen, L. Zhou, J. Qin, Y. Meng and T. Mu, *New J. Chem.*, 2020, **44**, 9493; (*c*) Y. Chen, D. Yu, L. Fu, M. Wang, D. Feng, Y. Yang, X. Xue, J. Wang and T. Mu, *Phys. Chem. Chem. Phys.*, 2019, **21**, 11810; (*d*) Y. Chen, D. Yu, Y. Lu, G. Li, L. Fu and T. Mu, *Ind. Eng. Chem. Res.*, 2019, **58**, 7308.

21 (*a*) M. Ilangovan, V. Guna, B. Prajwal, Q. Jiang and N. Reddy, *Carbohydr. Polym.*, 2020, **236**, 115996; (*b*) F. Luzi, D. Puglia, F. Sarasini, J. Tirillo, G. Maffei, A. Zuorro, R. Lavecchia, J. M. Kenny and L. Torre, *Carbohydr. Polym.*, 2019, **209**, 328; (*c*) R. Vijay, A. Vinod, D. L. Singaravelu, M. R. Sanjay and S. Siengchin, *Int. J. Lightweight Mater. Manuf.*, 2021, **4**(1), 43.

22 I. M. De Rosa, J. M. Kenny, D. Puglia, C. Santulli and F. Sarasini, *Compos. Sci. Technol.*, 2010, **70**(1), 116.

23 L. Hu, Z. Li, Z. Wu, L. Lin and S. Zhou, *Ind. Crops Prod.*, 2016, **84**, 408.

24 (*a*) P. Li, J. A. Sirvio, B. Asante and H. Liimatainen, *Carbohydr. Polym.*, 2018, **199**, 219; (*b*) A. Satlewal, R. Agrawal, S. Bhagia, J. Sangoro and A. J. Ragauskas, *Biotechnol. Adv.*, 2018, **36**(8), 2032.

25 P. Li, D. Cai, Z. Luo, P. Qin, C. Chen, Y. Wang, C. Zhang, Z. Wang and T. Tan, *Bioresour. Technol.*, 2016, **206**, 86.

26 K. Pakutsah and D. Aht-Ong, *Int. J. Biol. Macromol.*, 2020, **145**, 64.

27 N. H. A. Rahman, N. A. Ibrahim, B. W. Chieng and N. A. Rahman, *Polymers*, 2017, **9**(11), 588.

28 H. Wang, J. Li, X. Zeng, X. Tang, Y. Sun, T. Lei and L. Lin, *Cellulose*, 2019, **27**(3), 1301.

29 D. Hu, W. Ma, Z. Zhang, Y. Ding and L. Wu, *ACS Appl. Mater. Interfaces*, 2020, **12**(9), 11115.

30 Y. Xu, S. Yang, P. Zhao, M. Wu, X. Song and A. J. Ragauskas, *Carbohydr. Polym.*, 2021, **253**, 117253.

31 (*a*) Y. Chen, L. Pang, Y. Li, H. Luo, G. Duan, C. Mei, W. Xu, W. Zhou, K. Liu and S. Jiang, *Compos. Appl. Sci. Manuf.*, 2020, **135**, 105960; (*b*) T. Horseman, M. Tajvidi, C. I. K. Diop and D. J. Gardner, *Cellulose*, 2017, **24**(6), 2455.

32 N. Song, J. Yang, P. Ding, S. Tang and L. Shi, *Compos. Appl. Sci. Manuf.*, 2015, **73**, 232.

33 (*a*) H. A. Silvério, W. P. Flauzino Neto, N. O. Dantas and D. Pasquini, *Ind. Crops Prod.*, 2013, **44**, 427; (*b*) B. Soni, B. Hassan and B. Mahmoud, *Carbohydr. Polym.*, 2015, **134**, 581.

34 J. Wu, X. Du, Z. Yin, S. Xu, S. Xu and Y. Zhang, *Carbohydr. Polym.*, 2019, **211**, 49.

35 N. Yildirim and S. Shaler, *Materials*, 2017, **10**(7), 718.